Weak Boson Fusion $H \to WW^{(*)} \to l^+l^-p_T^{miss}$ as a search mode for an intermediate mass SM Higgs boson at ATLAS

C.M.Buttar[1], R.S.Harper[1], K. Jakobs[2]

[1]Dept. of Physics and Astronomy, University of Sheffield, UK

[2]Institut für Physik, Universität Mainz, Germany

December 19, 2002

ATL-PHYS-2002-033
19 December 2002

Abstract

The weak boson fusion production process gives a distinctive signature for a Standard Model Higgs boson due to forward tagging jets in the final state. The decay $H \to WW^{(*)} \to l^+l^-p_T^{miss}$ is studied as a discovery channel for an intermediate mass Higgs boson, and acceptance cuts are developed to isolate the signal from the main Standard Model backgrounds. The distinctive signature allows a signal to be observed above the 5σ level for $M_H = 150 - 190$ GeV with an integrated luminosity of 5 fb^{-1} and for $M_H = 130 - 190$ GeV with 10 fb^{-1}. A systematic uncertainty on the background rate of up to 10% is also considered, and is not found to adversely affect the discovery potential.

1 Introduction

The search for the origin of electroweak symmetry breaking is one of the primary tasks for the ATLAS experiment at the LHC. In the Standard Model there is one neutral scalar Higgs boson; its mass is not predicted by the theory but unitarity arguments impose an upper limit of ≈ 1 TeV, and direct searches at LEP have found a lower limit of 114.4 GeV at 95% confidence level [1]. Precision fits to electroweak data do, however, suggest a relatively small Higgs mass, $M_H < 193$ GeV at 95% C.L. [2], therefore the intermediate mass region is extremely important. Whilst the $H \to ZZ^{(*)} \to 4l$ channel has been studied extensively for this mass region [3], for $M_H \approx 170$ GeV the branching ratio of $H \to ZZ^*$ is suppressed as the $H \to WW$ decay mode opens up, causing a sharp decrease in the signal significance. Therefore the $H \to WW^{(*)} \to l^+l^-p_T^{miss}$ channel has been studied

as a discovery channel at the LHC [4]; since no mass peak can be reconstructed due to the presence of neutrinos in the final state an excess of events above the expected SM background must be observed. It was found that with an integrated luminosity of 30 fb^{-1} and a systematic uncertainty of 5% on the background rate a 5σ signal could be observed for $M_H = 150 - 190$ GeV.

Vector Boson Fusion (VBF) has the second largest production cross-section for an intermediate mass Higgs boson, and provides additional signal characteristics in the form of forward tagging jets from the scattered quarks. This has been studied for the $H \to WW^{(*)} \to e^{\pm}\mu^{\mp}p_T^{miss}$ decay channel at LHC energies with a parton level simulation [5] and was found to be a promising discovery channel for the mass range $M_H = 140 - 190$ GeV, with the ability to observe a signal at or above the 5σ level with an integrated luminosity of 5 fb^{-1}, equivalent to just 6 months low luminosity running. This work develops the analysis in Ref. [5] using PYTHIA for parton showering and hadronisation, and ATLFAST to simulate the response of ATLAS. The $H \to WW^{(*)} \to (e^+e^-/\mu^+\mu^-)p_T^{miss}$ channel is also investigated, which was not considered in [5]. The combined discovery potential of WBF $H \to WW^{(*)} \to l^+l^-p_T^{miss}$ is then discussed, including the effect of a systematic uncertainty on the background rate.

2 Signal and Backgrounds

The signal process considered is a SM Higgs boson produced via WBF, $qq \to qq(WW, ZZ) \to qqH$, followed by the decay $H \to WW^{(*)} \to l^+l^-p_T^{miss}$. Therefore the basic signal consists of events with two (or more) jets, two leptons and missing transverse momentum due to the undetected neutrinos. The $e^{\pm}\mu^{\mp}p_T^{miss}$ and $(e^+e^-/\mu^+\mu^-)p_T^{miss}$ final states are considered separately in Sections 4 and 5 respectively, since additional background processes must be considered for the latter.

The production cross-section and $\sigma \cdot$ BR for $H \to WW^*$ for $120 < M_H < 190$ GeV are given in table 1. They were calculated to leading order using VV2H [6] and HDECAY [7]. Leading order values were used although next-to-leading order results are available [8] and show a 10% increase in cross-section, since many of the background processes are known only to leading order.

m_H (GeV)	120	130	140	150	160	170	180	190
$\sigma(qqH)$ (pb)	4.36	4.04	3.72	3.46	3.22	3.06	2.82	2.64
$\sigma \cdot BR(H \to WW^{(*)})$ (fb)	531	1127	1785	2370	2955	2959	2620	2054

Table 1: Total vector boson fusion production cross-sections $\sigma(qqH)$ and $\sigma \cdot BR(H \to WW^{(*)})$ and as a function of the Higgs boson mass.

The dominant gg-production process was also found to contribute to the signal, where

ISR and FSR jets fulfil the tagging jet criteria. For both the $e\mu$ and $ee/\mu\mu$ channels the following processes have been considered as backgrounds.

- The dominant physics background comes from $t\bar{t}+jets$ production, since the cross-section is large and the branching ratio BR$(t \to Wb) \approx 1$. Leptonic decays of the W's then give a final state similar to the signal. Single top production in association with a W, where both the top and W decay leptonically, must also be considered.
- WW production in association with two or more jets is another source of background events. Both electroweak (EW) processes, occurring through the exchange of an electroweak boson, and QCD processes, occurring through the exchange of a quark or gluon, are considered.
- Drell-Yan production of $\tau^+\tau^-$ is also considered, as leptonic decays of the taus can be misidentified as leptonic W decays. Again both EW and QCD processes are considered.

For the $ee/\mu\mu$ channel additional backgrounds from lepton pair-production processes must also be considered.

- The dominant pair-production background comes from the Drell-Yan production of process $e^+e^-/\mu^+\mu^-$ in association with two or more jets, which has a large cross-section at the LHC.
- Additional pair-production background comes from ZZ processes. There are two possibilities to consider here; firstly, where one Z decays to an $e^+e^-/\mu^+\mu^-$ pair and the other hadronically to give jets, secondly where one Z again decays to an $e^+e^-/\mu^+\mu^-$ pair, and the other to neutrinos, with two jets coming from additional radiation.

The $\sigma \cdot$ BR for the main backgrounds are given in table 2.

An additional source of background that has not been considered can arise from $b\bar{b}$ production which has a huge cross-section at the LHC, of order 500 μb, however it has been demonstrated that this is negligible for signatures where the dominant background is $t\bar{t}$ [9]. Furthermore, the $b\bar{b}$ background was considered statistically in Ref. [10] and was found to have a cross-section of order 1 fb for two isolated, high-p_T leptons before other cuts. This is much smaller than the signal cross-section.

process	p_T-cutoff	cross-section
$\gamma^*/Z\ + jets, \gamma^*/Z \to \ell\ell$	> 10 GeV	5227 pb
$t\bar{t}$		55.0 pb
QCD $WW + jets$		16.7 pb
$qg \to Wt$		4.8 pb
EW $\tau\tau + jets$		170.8 fb
EW $WW + jets$		81.6 fb

Table 2: *Cross-sections times leptonic branching ratios ($W \to l\nu$, $l = e, \mu$ and τ) for the major background processes. All backgrounds except the electroweak WW and $\tau\tau$ + jet background have been computed using the PYTHIA Monte Carlo programme.*

3 Event Generation

Events are generated using the PYTHIA 6.1 [11] Monte Carlo. Initial and Final State Radiation (ISR and FSR), fragmentation and decay and multiple interactions are all used, with the CTEQ5L parameterisation of the parton distribution functions [12]. Some processes are not included in PYTHIA. Single top production was generated using the Onetop generator [13] interfaced to PYTHIA and ATLFAST. The two EW processes are not included in PYTHIA and were generated by interfacing a parton level simulation, which produced $WW + 2j$ or $\tau\tau + 2j$ events, to PYTHIA, which was then used to perform ISR, FSR, fragmentation and decay and multiple interactions[1]. The ATLFAST [14] package has been used with default settings to perform a detector simulation.

The channels are triggered by the single or di-lepton trigger. High trigger efficiencies can be reached using the ATLAS trigger thresholds [15] for a single electron or muon with P_T values greater than 25 GeV/c and 20 GeV/c respectively. However, although the trigger acceptance for electrons is $|\eta| < 2.5$, for the muons it is $|\eta| < 2.2$. The reduced muon trigger coverage compared to the offline cuts introduces an acceptance loss of 2%, which is included in the results presented.

4 The $H \to WW^{(*)} \to e^{\pm}\mu^{\mp}p_T^{miss}$ channel

First the $e\mu$ final state is investigated, which has the advantage of different flavour leptons in the final state so that lepton pair-production backgrounds need not be considered. The acceptance cuts proposed in Ref. [5] were used as a starting point then a multivariate optimisation performed to find the best combination of values for the cuts. This optimisation was performed independent of the Higgs boson mass for $150 < M_H < 180$ GeV so as not to bias the acceptance cuts towards a particular value of M_H.

[1] Parton level code provided by D.Zeppenfeld. Interface written by R.Mazini.

The final state of the signal at leading order contains one electron and one muon from the decay of the W bosons. These are required to be observed in the detector and trigger the experiment. Therefore one isolated electron and one isolated muon must be found which satisfy

Lepton Acceptance

$$p_T^{l1} \geq 20.0 \text{ GeV} \;\; p_T^{l2} \geq 15.0 \text{ GeV} \;\; |\eta_l| \leq 2.5$$

Next the candidate tag jets are searched for over the full calorimeter coverage ($|\eta| < 4.9$). The measured jet energies are corrected back to the original parton energy and the highest P_T jet in each of the positive and negative regions of pseudorapidity are taken as the tag jet candidates. Studies have shown that this choices has a high efficiency for correctly identifying the tag jets. For a Higgs boson of mass 160 GeV and jet p_T threshold of 20 GeV this selects the correct tag jets in 86%. The efficiency of this tagging definition is higher than alternative choices based on highest energy, largest pseudo-rapidity separation or the minimum p_T imbalance between the Higgs boson and the tag jet system.

As the tag jets are produced in an electroweak process, the differences between their characteristics and those of the QCD backgrounds can be exploited. For the signal the incoming quarks have relatively high energy and are then scattered by the emission of W or Z bosons, which tend to take a small fraction of the quark energy. Their transverse momentum, though, is of order M_W. The final state quarks therefore have relatively large energy and modest transverse momentum, so the scattering angle with respect to the beam-line is small and the resulting jets will be found in the forward regions of the detector. In contrast, the dominant QCD background processes tend to have centrally produced jets. The η distributions of identified tag jets for the signal and in the $t\overline{t}$ background are shown in figure 1. This shows that a cut on the difference in η for the tagging jets, $\Delta\eta_{j1j2}$, will be very effective, the distribution is shown in figure 1.

Once the candidate tag jets are identified they must satisfy:

Forward Tagging

$$p_T^{j1} \geq 40.0 \text{ GeV} \;\; p_T^{j2} \geq 20.0\text{GeV} \;\text{ and }\; \Delta\eta_{j1j2} > 3.8$$

The tag jets are not expected to be b-jets, and therefore a b-veto is applied to tagging jets within the central tracking region ($|\eta| < 2.5$). This rejects $t\overline{t}$ events where one of the b-quarks is identified as a tagging jet. The maximum signal significance was found for a b-jet efficiency of 0.7, giving a mis-tag probability of 0.25 for c-quark jets and 0.04 for light quark and gluon jets.

The leptons were then required to be in the pseudorapidity gap spanned by the two tagging jets.

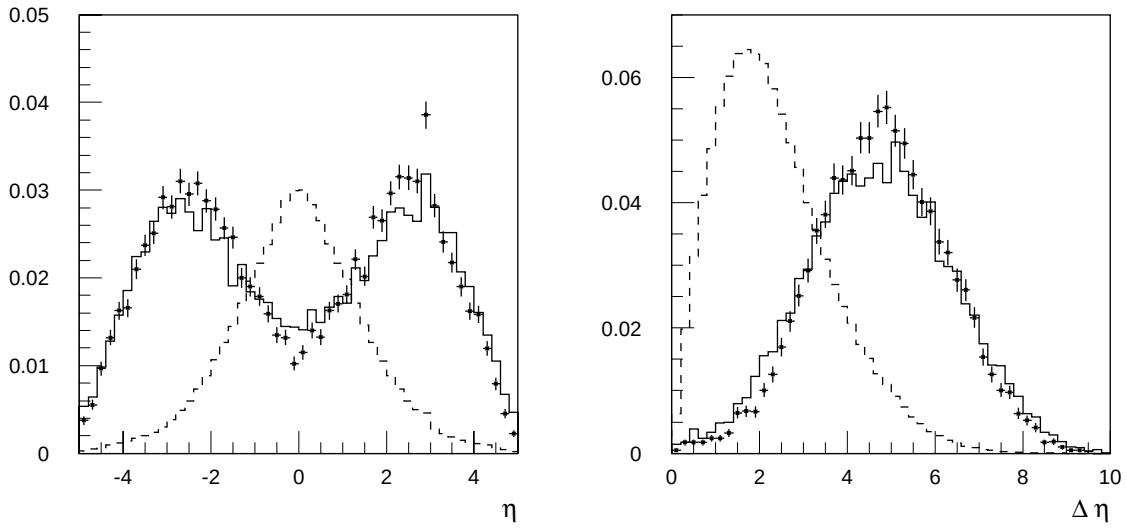

Figure 1: *Pseudorapidity distribution (left) and separation* ($\Delta\eta$) *between the tag jets (right) in signal events* ($M_H = 160$ *GeV). The full histograms show the distributions at parton level, the dots corresponds to the reconstructed distributions, after the tagging algorithm has been applied. The corresponding distributions for jets identified as tag jets in* $t\bar{t}$ *events are superimposed as dashed histograms. All distributions are normalized to unity.*

The efficiency of the reconstructed tagging jets in the presence of pile-up has been investigated using a GEANT based full simulation of ATLAS [16]. Differences were found in the efficiencies calculated using ATLFAST and the full simulation in the transition regions between calorimeters and in the forward region, these were parametised as a function of P_T and η, and used to correct the fast simulation results.

Another characteristic feature of this channel is the anti-correlation of the W spins from the decay of the scalar Higgs boson. In the rest frame of the Higgs boson the W's are produced almost at threshold for $M_H < 2M_W$ and the lepton and neutrino from each W decay are emitted back-to-back with equal energy. When the W^+ decays into an anti-lepton and a neutrino the anti-lepton is preferentially emitted in the same direction as the W^+ spin. Similarly the lepton from the decay of the W^- is preferentially emitted in the opposite direction to the W^- spin. Therefore since the W^+ and W^- have opposite spins the lepton and anti-lepton tend to be emitted in the same direction, and this characteristic remains when boosted back to the lab frame since $M_H \approx 2M_W$. A series of cuts are performed on the angular separation of the charged leptons, namely the azimuthal opening angle $\Delta\phi$, the cosine of the polar opening angle $\cos\theta_{ll}$ and the separation in the lego plot ΔR_{ll}. Also, the invariant mass of the visible leptons M_{ll} is limited to $M_H/2$, as in the rest frame of the Higgs the di-lepton system and neutrino system are emitted back-to-back and with equal energy. A cut on the maximum di-lepton invariant mass is therefore applied.

Finally, a cut is also applied on the maximum lepton transverse momentum. Plots of $\Delta\phi$ and M_{ll} for the the signal and background distributions are shown in figure 2.

Lepton Angular Cuts

$$\Delta\phi \leq 1.05$$

$$\cos\theta_{ll} \geq 0.2 \;\; ; \;\; \Delta R_{ll} \leq 1.8$$

$$M_{ll} \leq 85 \text{ GeV} \;\; ; \;\; p_{T,l} \leq 120 \text{ GeV}$$

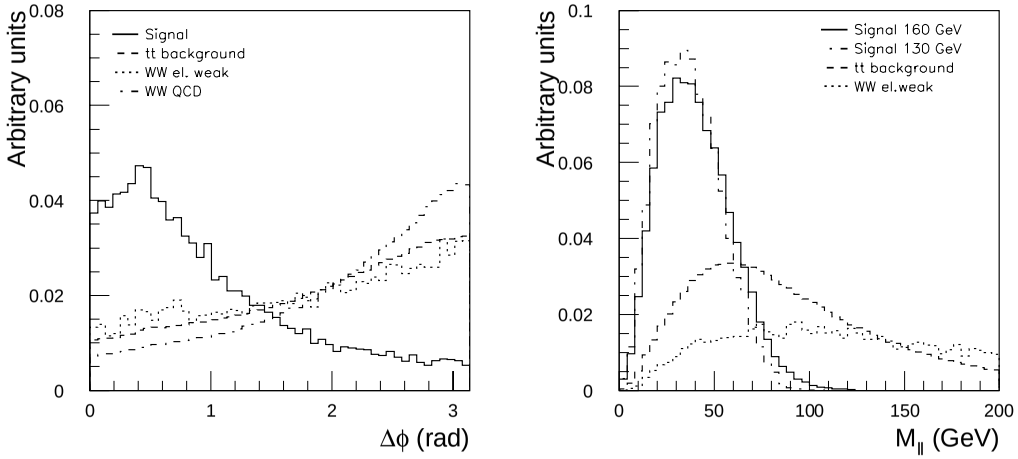

Figure 2: *Azimuthal opening angle of leptons (left) and di-lepton invariant mass (right) for signal with* $M_H = 160$ *and* $t\bar{t}$ *and EW and QCD WW backgrounds.*

A reduction in the $\tau\tau + jets$ background arising from Z+jet events in which the Z decays to τ-pairs can be achieved by reconstructing the $\tau\tau$ system using the collinear approximation. In Z+jet events, the Zs are typically produced with sufficiently high P_T resulting in large boosts to the taus. The τ-decay products are then approximately collinear in the laboratory frame, the τ-momentum can then be reconstructed from the observed decay products and the missing transverse momentum [17]. The fraction of energy $x(\tau_1)$ and $x(\tau_2)$ taken by the charged lepton from the decay of each τ can be found, and for real $\tau\tau$ pairs these both tend to take values between 0 and 1. This is not the case for the signal, however, where either $x(\tau_1)$ or $x(\tau_2)$ will usually take a negative value. Additionally, the reconstructed invariant mass of real $\tau\tau$ pairs will peak at M_Z since the dominant process is $Z \to \tau\tau$. Therefore events are vetoed that satisfy the following:

Real Tau Rejection

$$x_{\tau_1}, x_{\tau_2} \geq 0.0 \;\; ; \;\; M_Z - 25 \geq M_{\tau\tau} \geq M_Z + 25 \text{ GeV}$$

A further consequence of the tag jets being high energy and widely seperated is that the invariant mass of the tag jets will be relatively large compared with the QCD background processes. Therefore a cut is applied on the minimum invariant mass of the tag jets, M_{jj}.

Tagging jet mass

$$M_{jj} > \ 550 \text{ GeV}$$

In the absence of initial and final state radiation, the transverse momentum of the Higgs should be balanced by the transverse momentum of the tagging jets, the P_T^{tot} distribution for signal and background are shown in figure 3. A cut is applied to the total event P_T^{tot}, defined as:

$$\vec{P}_T^{tot} = \vec{P}_T^{l,1} + \vec{P}_T^{l,2} + \vec{P}_T^{miss} + \vec{P}_T^{j,1} + \vec{P}_T^{j,2}$$

Transverse momentum balance

$$|\vec{P}_T^{tot}| < 30 \text{ GeV}$$

In the weak boson fusion process the interaction between the initial state quarks proceeds through the exchange of weak bosons, which do not carry colour. Any additional hadronic radiation from the signal process can only come from gluons radiated from the initial or final state quarks; it is therefore most likely to be found in the forward and backward regions of the detector. The dominant QCD backgrounds, on the other hand, proceed by the exchange of colour between the initial state partons and additional hadronic radiation is more likely to be emitted into the central region. Therefore a central jet veto is applied, where events are vetoed when one or more jets are found that satisfy the following criteria:

Central Jet Veto

$$\text{no jets with } P_T > 20 \text{ GeV in the range } |\eta| < 3.2$$

The Drell-Yan production is a serious background for the $ee/\mu\mu$ channel. However, it can also contribute to the $e\mu$ signal at lower rates through the Drell-Yan production of τ-pairs where both taus decay leptonically. Most of the Z-component has already been rejected by the cut on M_{ll} but the γ^* component requires an additional cut. This can be achieved by cutting on the transverse mass of the $ll\nu$ system, defined by:

$$M_T(ll\nu) = \sqrt{2P_T(ll)P_T^{miss}(1 - cos\Delta\phi)}$$

where $\Delta\phi$ is the angle between the di-lepton vector and the P_T^{miss} vector in the transverse plane. The distribution of $M_T(ll\nu)$ is shown in figure 3. In order to reject $\tau-$decays that mimic the signal, a cut on $M_T(ll\nu)$ is made:

Tau decays

$$M_T(ll\nu) > 30 \text{ GeV}$$

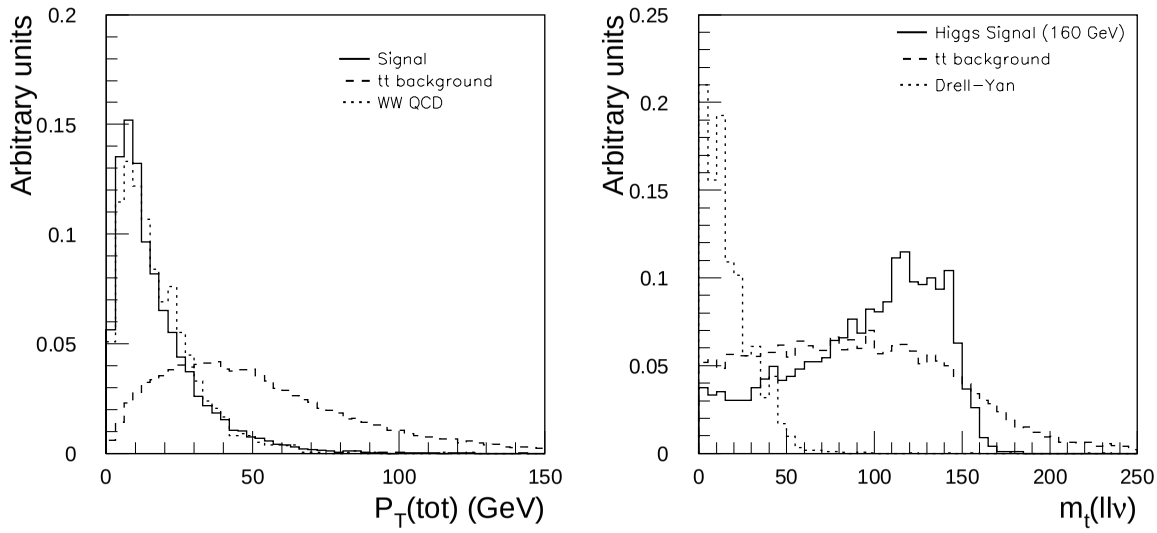

Figure 3: *Distribution of the momentum balance* $|\vec{P}_T^{tot}|$ *between the reconstructed leptons,* P_T^{miss} *and the tag jets (left) and distribution of the transverse mass* $M_T(ll\nu)$ *of the dilepton and neutrino system (right) for signal events with* $M_H = 160$ *GeV and for various backgrounds.*

The signal and background cross-sections for the different steps of the analysis are shown in table 3. The results show that the gg-channel contributes around 10% of the signal. The tagging jet cut strongly suppresses all the backgrounds, but is particularly effective at suppressing the QCD backgrounds. The lepton cuts and P_T balance cuts suppress both the QCD and EW backgrounds. The QCD backgrounds are further suppressed by the jet-veto and jet-mass cuts. After the jet-veto cut the QCD backgrounds are at a similar level to the EW backgrounds, the largest remaining background being the $\tau\tau$+jets. This effectively is suppressed by the $M_T(ll\nu)$ cut. The remaining background arises from $t\bar{t}$ and single top production (0.51 fb and 0.15 fb respectively) due to its very large production cross-section and the electroweak WW+jets background which are very similar to the signal.

The top section of table 3 is based on direct electrons and muons from the W-decays. However, an additional signal arises from the detection of electrons and muons from cascades of $W \to \tau\nu \to e/\mu + X$. The contributions to the signal have been calculated for both the e/μ channel and the $ee/\mu\mu$ channels and are included in the final results given in table 3.

	signal (fb)		background (fb)					
	VV	gg	$t\bar{t} + Wt$	$WW + jets$		$\tau\tau + jets$		total
				EW	QCD	EW	QCD	
Lepton acceptance	29.6	121.9	6073	14.2	590.5	5.96	25222	31906
+ Forward Tagging	11.4	2.24	127.5	8.01	1.41	1.55	208.3	346.8
+ Lepton angular cuts	6.95	1.36	17.0	0.54	0.17	0.50	30.0	48.2
+ τ rejection	6.64	1.34	16.3	0.50	0.17	0.09	5.93	23.0
+ Jet mass	5.30	0.76	10.0	0.50	0.06	0.09	4.01	14.6
+ P_T^{tot}	4.52	0.50	2.34	0.38	0.04	0.07	2.70	5.53
+ Jet veto	3.87	0.34	0.72	0.34	0.03	0.07	1.70	2.86
+ M_T-cut	3.76	0.31	0.66	0.32	0.02	0.01	0.03	1.04
$H \to WW \to e\mu + X$ incl. $\tau \to e, \mu$ contr.	4.32	0.33	0.75	0.35	0.03	0.01	0.03	1.17
$H \to WW \to ee/\mu\mu + X$ incl. $\tau \to e, \mu$ contr.	3.92	0.30	0.71	0.36	0.04	0.04	0.12	1.28

Table 3: *Accepted signal (for $M_H = 160$ GeV) and background cross-sections in fb for the $H \to WW \to e\mu$ channel after the application of successive cuts. For the signal the contributions via the vector boson fusion and the gluon fusion channel are given separately. The last two lines give the final numbers if the contributions from $W \to \tau\nu \to l\nu\nu\ \nu$ are added for both the $e\mu$ and the $ee/\mu\mu$ final states.*

5 The $H \to WW^{(*)} \to (e^+e^-/\mu^+\mu^-)p_T^{miss}$ channel

Next the signal from same-flavour leptons is investigated; as mentioned earlier additional lepton pair-production backgrounds must be included. As discussed in section 2 there are additional backgrounds arising from ZZ and γ^*/Z backgrounds. The analysis is started by applying the same cuts as developed for the $e\mu$ channel. The on-shell ZZ background is largely suppressed by the e/μ cuts, but additional cuts are required to suppress the off-shell γ^*/Z background.

There are several features of the Z/γ^* background that may allow it to be distinguished from the signal. Firstly, for $Z \to ee/\mu\mu$ events the di-lepton invariant mass M_{ll} should mostly fall around the Z mass, whereas for most of the $\gamma^* \to ee/\mu\mu$ events the di-lepton invariant mass will be relatively small. The majority of the $Z \to ee/\mu\mu$ events are rejected by the cut of $M_{ll} < 90$ GeV applied during the lepton angular cuts. A more stringent cut requiring $M_{ll} < 75$ GeV is applied to eliminate most of the background events with M_{ll} around the Z mass with a negligible effect on the signal. However, the majority of the M_{ll} distribution for the Z/γ^* background takes lower values, consistent with being from $\gamma^* \to ee/\mu\mu$ events, but the signal has a very similar distribution. Thus, there is no

opportunity for further background reduction.

Secondly, since there are no neutrinos in the final state for the Z/γ^* process a smaller amount of missing transverse momentum is expected compared to the signal process, which has two neutrinos in the final state. The tendency for much lower missing transverse momentum in Z/γ^* events is, therefore applying a cut on the minimum p_T^{miss} should eliminate a large proportion of this background whilst leaving the signal largely untouched. The $ee/\mu\mu$ *cuts* are therefore defined as

$ee/\mu\mu$ *cuts*

$$M_{ll} \leq 75 \text{ GeV} \;\; ; \;\; p_T^{miss} \geq 30 \text{ GeV}$$

The numbers for signal and background presented in this report are different from those presented in the original parton level study [5]. The main difference has been found to be a reduced signal efficiency due to a lower lepton acceptance and a lower efficiency for reconstructing tag jets. Both these effects are due to initial and final state gluon radiation which reduces the lepton isolation and produces non-gaussian tails in the jet response. However this note confrims the conclusion of Ref. [5] that vector boson fusion is a powerful intermediate mass Higgs discovery channel at the LHC.

6 Systematic uncertainties for the $H \rightarrow WW$ channels

The QCD backgrounds quoted in the previous section have all been calculated using the PYTHIA parton shower Monte Carlo. Due to the requirement of two hard tag jets in the final state the final number of predicted background events is sensitive to the hard tail of the jet distribution in $t\bar{t}+$ jet or $WW + jet$ events.

In order to get an estimate of the systematic uncertainties in the QCD background predictions, the dominant $t\bar{t} + jet$ background has also been evaluated using explicit matrix element calculations for $t\bar{t} + 0\ jet$, $t\bar{t} + 1\ jet$ and $t\bar{t} + 2\ jet$ final states. These matrix element calculations have been provided by the authors of Ref. [5] and have been interfaced to the PYTHIA generator. In order to avoid double counting when adding the three contributions the procedure proposed in Ref. [5], to define three distinct final state jet topologies, has been adopted. For $t\bar{t}\ + 0\ jets$ only the two b-jets are considered as tag jet candidates. Initial and final state radiation in these events may lead to a rejection of the event due to the jet veto. A distinctively different class is defined by those $t\bar{t}\ + 1\ jet$ events where the final state light quark or gluon gives rise to one tag jet and one of the two

b-jets is identified as the other tag jet. Finally, a third class is defined where in $t\bar{t} + 2\ jets$ the final state light quarks or gluons are identified as tag jets.

The three final state topologies have been simulated separately in PYTHIA, without inital and final state radiation. In the generation a parton level cutoff of 10 GeV has been introduced to regulate the divergencies appearing in the tree level matrix elements. The cross sections at generation (multiplied by the branching ratio for W decays into electrons and muons) as well as after various cuts are given in Table 4. The PYTHIA predictions, using the same tagging definitions as for the matrix element calculation, are also given in Table 4 for comparison .

	$t\bar{t}$ + 0 jet	$t\bar{t}$ + 1 jet	$t\bar{t}$ + 2 jets
Tree level cross sections	20300 fb	57300 fb	84200 fb
Leptons + Tag jets	7.06 fb	140.33 fb	152.49 fb
+ Lepton angular cuts, Tau rejection and Jet mass	0.10 fb	12.45 fb	16.96 fb
+ P_T^{tot}	0.10 fb	3.62 fb	2.42 fb
+ Jet veto	0.03 fb	0.78 fb	0.25 fb
PYTHIA prediction	0.04 fb	0.40 fb	0.07 fb

Table 4: Accepted cross sections for the $t\bar{t}$ + 0,1 and 2 jet tree level matrix element calculations, and the prediction from PYTHIA.

The large cross sections for $t\bar{t} + 1\ jet$ and $t\bar{t} + 2\ jet$ demonstrate that the perturbative approach breaks down. Already for a P_T cutoff of 40 GeV, which is larger than the jet definition threshold of 20 GeV, the higher order tree level cross sections are comparable to the $t\bar{t}$+ 0 jet cross section. The accepted cross sections after applying all cuts including the cut on the transverse momentum balance have finally to be multiplied with the jet veto efficiencies. These efficiencies have been evaluated from the PYTHIA parton shower simulation discussed above. For that purpose the parton shower events have been split into three categories, depending on the number of b-jets used as tag jets. Since in $t\bar{t}$ events the b-jets from the t-decays can also set the central jet veto, the veto efficiencies depend on the final state topology. In $t\bar{t} + 1\ jet$ and $t\bar{t} + 2\ jet$ events the veto can be either set by a b-jet not used as tag jet or by jets from initial or final state radiation. After the corresponding efficiency factors for the three classes are applied the accepted cross sections as given in the last row of Table 4 have been obtained. As discussed in Ref. [5] and in agreement with the PYTHIA parton shower simulation, the dominant contribution arises from configurations where one tag jet is a b-jet and the other one originates from an emitted parton in the $t\bar{t} + 1\ jet$ process.

If these cross sections are added the total $t\bar{t}$ background is estimated to be 1.08 fb, which is a factor of 2.1 higher than the value determined with the PYTHIA parton shower approach. This simple addition may overestimate the true $t\bar{t}$ background since the divergencies in the tree level calculations are not compensated for by P_T dependent topological K-factors, which may take values smaller than 1 in the low P_T region. Therefore, this estimate is used in the evaluation of the signal significance as a conservative estimate of the $t\bar{t} + jet$ background.

Given these major uncertainties to predict the absolute level of the $t\bar{t}$ background, it is important to determine this background directly in the experiment. As mentioned already above, no mass peak can be reconstructed and evidence for a signal must be claimed from an excess of events after all cuts. Although the shape of the background is not very pronounced, most background events lie in the same region of transverse mass as the signal. The dominant background is the $t\bar{t}$+ jet background. It is expected that at least the shape of this background can be determined from $t\bar{t}$ events observed at the LHC. In $t\bar{t}$ events one may require only one leptonic decay and reconstruct the second top decaying into three jets. After requiring the forward jet tag criteria in addition, and correcting for differences in reconstruction efficiencies, this should provide an absolute prediction of the background rate with smaller uncertainties.

In addition, the selection cuts can be varied. An interesting approach is, for example, to apply all cuts discussed above except the *lepton angular cuts*. The distribution of the reconstructed transverse mass M_T is shown for a Higgs boson signal with $m_H = 160$ GeV above the backgrounds in Fig. 4 with (a) and without (b) applying the lepton angular cuts. Even if no lepton cuts are applied an impressive signal can be seen above a background which extends to large M_T values. The background in the high M_T region can be used to perform a normalization outside of the signal region and to predict the background below the signal peak, if the shape of the distribution is taken from a Monte Carlo prediction. Already for an integrated luminosity of 10 fb^{-1} a statistical uncertainty of about 10% for the predicted background can be reached. In addition, as discussed in the following section, the distribution of the azimuthal difference between the two leptons, $\Delta\phi$, can be used to extract a background normalization for events below the signal peak. Given these additional possibilities, it is assumed in the following that the total background rate can be determined with an uncertainty of $\pm 10\%$.

7 Evidence for a spin-0 resonance in $H \to WW^{(*)}$

As discussed above, the di-lepton azimuthal angular separation is sensitive to the spin of the Higgs. By making the selection without the lepton cuts an unbiased distribution

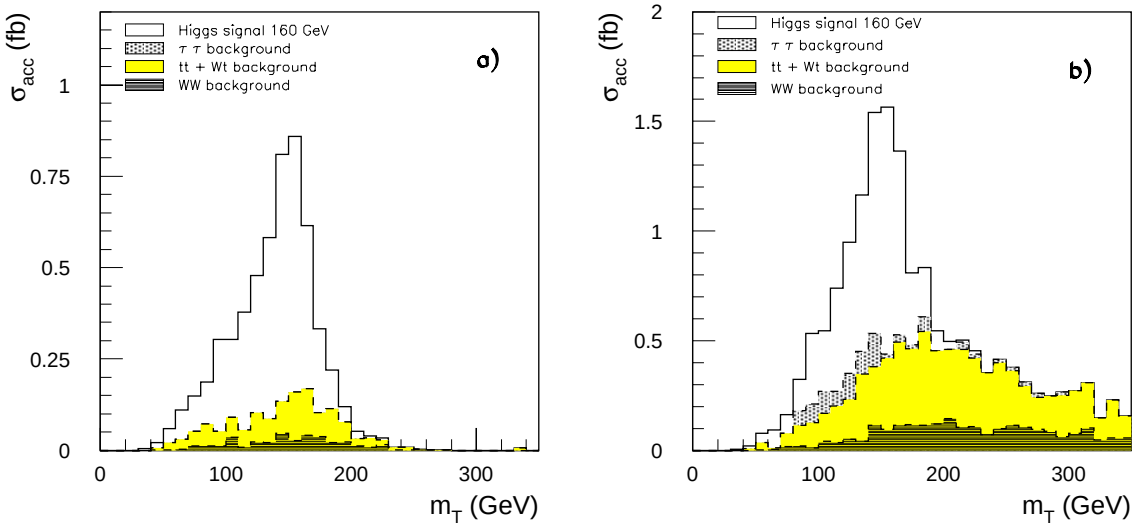

Figure 4: *Distributions of the transverse mass M_T for a Higgs boson signal of 160 GeV above the sum of the various backgrounds (a) after applying all cuts and (b) all cuts except the lepton angular cuts. The accepted cross-sections $d\sigma/dM_T$ (in fb/10 GeV) including all efficiency and acceptance factors are shown in both cases. The number of events observed in the detector can be obtained by multiplying by the integrated luminosity.*

of the azimuthal difference $\Delta\phi$ between the two leptons can be reconstructed. In Fig. 5 this distribution is shown for the events passing all cuts except the lepton angular cuts selected in two different regions of M_T, in the so called signal region ($M_T < 175$ GeV) and in a control region ($M_T > 175$ GeV). For events in the signal region the observed distribution is consistent with the existence of a spin-0 resonance above a flat background. The pronounced structure at small $\Delta\phi$ is not present for events in the control sample, where the $t\bar{t}$ and WW backgrounds are expected. The unbiased $\Delta\phi$ distribution in the signal region can therefore be used for both a demonstration of the consistency of the signal with a spin-0 hypothesis and for an additional background normalization. This normalization can be performed in the high $\Delta\phi$ region directly from events below the peak.

8 Results

The analysis described above was carried out for 110 GeV $< M_H <$ 190 GeV. As there is no distinct mass peak due to the neutrinos in the final state, the signal significance was calculated using a transverse mass window. Below the WW-threshold the optimum mass

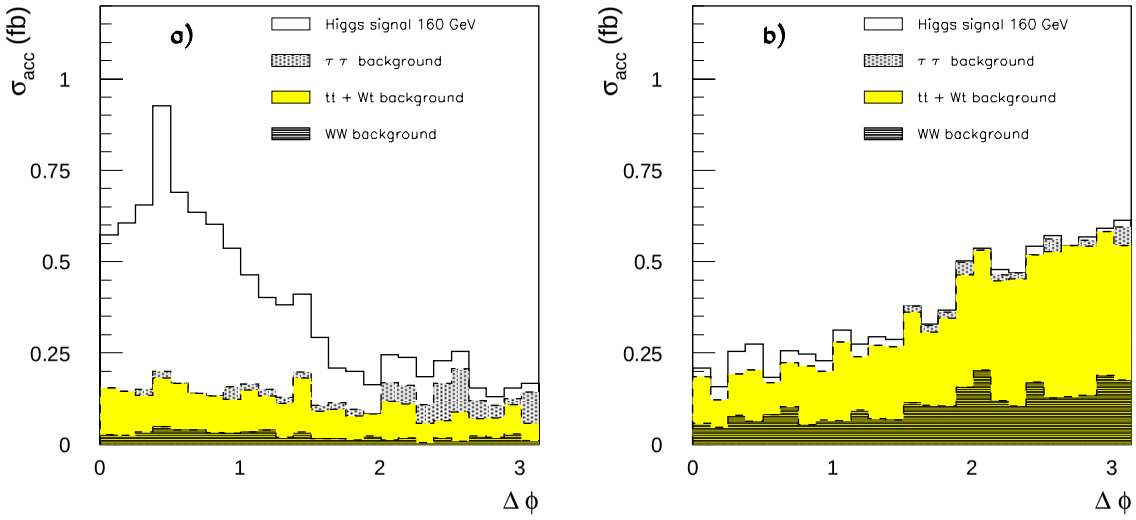

Figure 5: *Distributions of the azimuthal opening angle $\Delta\phi$ between the two leptons for (a) events in the signal region ($M_T < 175$ GeV) and (b) outside the signal region ($M_T > 175$ GeV). The accepted cross-sections $d\sigma/dM_T$ (in fb/10 GeV) including all efficiency and acceptance factors are shown in both cases. The number of events observed in the detector can be obtained by multiplying by the integrated luminosity.*

window that maximised S/B was found to be $50 < M_T < M_H + 10$ GeV, as shown in figure 6 this reconstructs most of the signal in the high S/B region. Above the WW-threshold the upper limit of the mass window was optimised using the signal and background distributions for each Higgs mass. The results are given in table 5. The e/μ channel has a S/B > 1 for $M_H > 130$ GeV, while the $ee/\mu\mu$ channel has S/B > 1 for $M_H > 140$ GeV. As discussed in section 6, the $t\bar{t}$-background from PYTHIA is 2.1 times lower than that calculated using PYTHIA interfaced to matrix elements. Although it is likely that the ME calculations and the simple addition of the three tree level cross-sections overestimate the background, to be conservative we have used the higher matrix element value. The statistical significance for 5 fb^{-1} was calculated using Poisson statistics because of the small number of events, and assuming a 10% systematic uncertainty on the background. A 5σ discovery can be claimed for a Higgs mass in the range $155 < M_H < 175$ GeV with 5 fb^{-1} of data for the e/μ channel alone, increasing to $150 < M_H < 190$ GeV when the $ee/\mu\mu$ channel is included. With 10 fb^{-1} of data the discovery range increases to $130 < M_H < 190$ GeV using both channels.

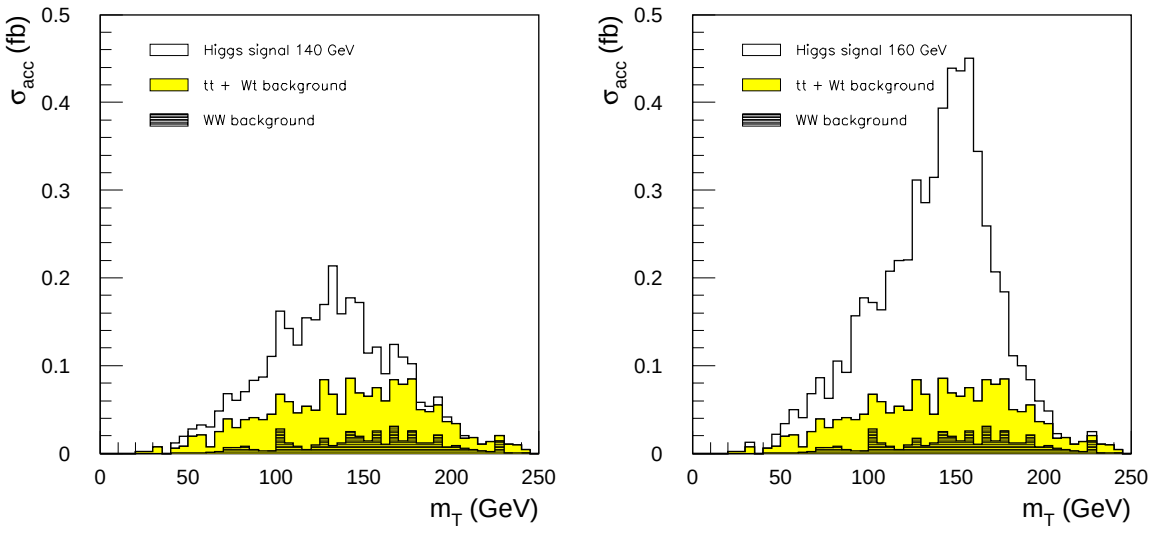

Figure 6: *Distributions of the transverse mass M_T for Higgs boson signals of 140 GeV (left) and 160 GeV (right) after all cuts are applied. The accepted cross-sections $d\sigma/dM_T$ (in fb/5 GeV) including all efficiency and acceptance factors are shown in both cases. The number of events observed in the detector can be obtained by multiplying by the integrated luminosity.*

9 Summary and Conclusions

This analysis demonstrates that Higgs production via W-boson fusion, $H \to WW^{(*)} \to l^+l^-p_T^{miss}$, is a robust discovery channel for an intermediate mass Higgs, with a 5σ discovery range of $150 < M_H < 190$ GeV for 5 fb^{-1}of data corresponding to only about 6 months of low luminosity data taking. The distinctive signature leads to a S/B>1 over the mass range $130 < M_H < 190$ GeV, large backgrounds such as $t\bar{t}$ being strongly suppressed by identifying the tagging jets associated with the WW-fusion. The other remaining significant background is the EW WW+jets process, which mimics the signal. Although there is no distinctive mass peak, and therefore this is a counting experiment, the significance is largely insensitive to uncertainties in the background at the level of 10%. The sensitivity of the di-lepton angular distribution to the spin of the Higgs can be used to confirm the spin-0 nature of the Higgs.

m_H (GeV)	110	120	130	140	150	160	170	180	190
Upper M_T bound for mass window (GeV)	120	130	140	150	160	175	190	220	240
$H \to WW \to e\mu + X$									
Signal ($10\ \text{fb}^{-1}$)	1.0	3.8	9.3	16.3	26.2	42.5	42.7	35.6	27.8
Background ($10\ \text{fb}^{-1}$)	4.9	5.9	6.9	8.1	9.8	12.4	13.8	16.3	17.1
Stat. significance ($10\ \text{fb}^{-1}$)	-	1.2	2.8	4.2	6.0	8.1	7.8	6.3	5.0
$H \to WW \to ee/\mu\mu + X$									
Signal ($10\ \text{fb}^{-1}$)	0.8	3.3	8.6	16.4	27.8	40.2	44.8	36.0	25.9
Background ($10\ \text{fb}^{-1}$)	6.1	7.4	8.9	10.0	12.2	14.3	15.9	18.4	19.2
Stat. significance ($10\ \text{fb}^{-1}$)	-	1.0	2.3	3.9	5.8	7.4	7.7	6.1	4.5

Table 5: Expected signal and background rates and signal significance for the three $WW^{(*)}$ decay channels as a function of M_H assuming an integrated luminosity of 10 fb^{-1}. The signal significance has been computed using Poisson statistics and assuming a systematic uncertainty of 10% on the background.

References

[1] LEP Higgs Working Group, LHWG note/2002-01, http://lephiggs.cern.ch/LEPHIGGS/papers/index.html

[2] M. Grünewald, Electroweak Physics, Plenary talk, ICHEP02, Amsterdam, 2002.

[3] ATLAS Collaboration, *Detector and Physics Performance Technical Design Report*, CERN/LHCC/99-14 (1999).

[4] K.Jakobs and Th.Trefzger, ATLAS internal note ATL-PHYS-2000-015 (2000).

[5] D.L.Rainwater and D.Zeppenfeld, Phys. Rev. D60 (1999) 113004, hep-ph/9906218.

[6] M.Spira, VV2H programme, home.cern.ch/m/mspira/www/proglist.html.

[7] M.Spira et al., Comp. Phys. Comm. 108 (1998).

[8] T.Han, G.Valencia and S.Willenbrock, Phys. Rev. Lett. 69 (1992) 3274.

[9] ATLAS Collaboration, ATLAS Detector and Physics Performance Technical Design Report, CERN/LHCC/99-15

[10] V.Cavasinni, D.Costanzo, ATLAS internal note ATL-PHYS-2000-013 (2000)

[11] T.Sjöstrand, Comp. Phys. Comm. 82 (1994).

[12] H.L.Lai et al., Eur. Phys. J. C12 (2000) 375.

[13] ONETOP: single top production Monte Carlo programme: http://www.pa.msu.edu/brock/atlas-ltop/EW-top-programs.html

[14] E.Richter-Was, D.Froidevaux, L.Poggioli, ATLAS internal note ATL-PHYS-98-131 (1998).

[15] ATLAS Collaboration, CERN/LHCC/2000-17 (2000)

[16] V.Cavasinni, D.Costanzo, I.Vivarelli, ATLAS internal note ATL-PHYS-2002-008 (2002).

[17] D.L.Rainwater, D.Zeppenfeld, K.Hagiwara, Phys. Rev. D59 (1999) 14037, hep-ph/9808468; T.Plehn, D.L.Rainwater and D.Zeppenfeld, Phys. Rev. D61 (2000) 093005.

[18] M.Dittmar and H.Dreiner, Phys. Rev. D55 (1997) 167.